

Exploring the Effect of Basis Rotation on NQS Performance

Sven Benjamin Kožić,^{1,*} V. Zlatić,¹ F. Franchini,¹ and S. M. Giampaolo^{1,†}

¹*Institut Ruđer Bošković, Bijenička cesta 54, 10000 Zagreb, Croatia*

(Dated: December 22, 2025)

Neural Quantum States (NQS) use neural networks to represent wavefunctions of quantum many-body systems, but their performance depends on the choice of basis, yet the underlying mechanism remains poorly understood. We use a fully solvable one-dimensional Ising model to show that local basis rotations leave the loss landscape unchanged while relocating the exact wavefunction in parameter space, effectively increasing its geometric distance from typical initializations. By sweeping a rotation angle ϕ , we compute quantum Fisher information and Fubini–Study distances to quantify how the rotated wavefunction moves within the loss landscape. Shallow architectures (with focus on Restricted Boltzmann Machines (RBMs)) trained with quantum natural gradient are more likely to fall into saddle-point regions depending on the rotation angle: they achieve low energy error but fail to reproduce correct coefficient distributions. In the ferromagnetic case, near-degenerate eigenstates create high-curvature barriers that trap optimization at intermediate fidelities. We introduce a framework based on an analytically solvable rotated Ising model to investigate how relocating the target wavefunction within a fixed loss landscape exposes information-geometric barriers—such as saddle points and high-curvature regions—that hinder shallow NQS optimization, underscoring the need for landscape-aware model design in variational training.

I. INTRODUCTION

Understanding the ground-state properties of quantum many-body systems remains a central challenge in statistical physics and quantum information theory. This difficulty originates from the exponential growth of the Hilbert space with system size, which renders exact representations of the state infeasible except for the smallest systems. While a limited number of models admit analytic solutions [4, 15], most physically relevant systems do not. Consequently, a wide range of approximate approaches has been developed, including Quantum Monte Carlo methods [6], tensor-network techniques [22], and density functional theory [17]. In addition to these well-established approaches, neural-network-based variational approaches are emerging as a powerful framework for representing quantum many-body states in recent years. Introduced by Carleo and Troyer [9], Neural Quantum States (NQS) encode the amplitudes of a quantum state through a parametrized neural network—most commonly a Restricted Boltzmann Machine (RBM)—whose parameters are optimized to approximate the ground state of a given Hamiltonian. This approach combines high representational flexibility with compatibility with stochastic optimization and variational Monte Carlo techniques. Unlike tensor networks, neural networks can, in principle, represent states with volume-law entanglement [13, 14, 24], and their training naturally benefits from parallelization and advances in machine-learning software and hardware [29].

Despite these advantages, the performance of NQS is known to depend strongly on the choice of basis used

to represent the quantum state. While basis dependence is an intrinsic feature of neural-network representations of a state [31], the mechanisms through which a change of basis impacts variational optimization remain poorly understood. In particular, it is unclear whether degraded performance under basis rotations should be attributed primarily to limitations in representational expressivity or instead to changes in the geometry of the optimization landscape encountered during training. Several recent works have also noted and investigated the issues related to basis dependency of NQS [11, 25, 31].

In this work, we investigate this issue within a controlled and analytically transparent framework, designed to disentangle physical effects from optimization artifacts. We employ shallow neural quantum state architectures—namely Restricted Boltzmann Machines and small feedforward networks—trained via stochastic reconfiguration (quantum natural gradient) [27]. Our analysis focuses on the one-dimensional transverse-field Ising model with periodic boundary conditions, considering both ferromagnetic ($J = -1$) and antiferromagnetic ($J = +1$) couplings. A site-resolved basis rotation, parameterized by an angle ϕ , is applied to the exact ground state, thereby modifying its representation in Hilbert space without affecting the Hamiltonian spectrum, entanglement properties, or underlying physical content. Therefore, within this framework, basis rotations act solely to reposition the exact ground state inside an otherwise unchanged loss landscape. As a consequence, the resulting optimization difficulties originate only from geometric effects. It depends on where the target state resides relative to typical initial variational states, rather than on any modification of the Hamiltonian or the variational objective. By sweeping the rotation angle ϕ , we explicitly follow the motion of the target state in parameter space, characterizing it through information-geometric measures such as the quantum Fisher information and

* skozi@irb.hr

† sgiampa@irb.hr

the Fubini–Study distance, which quantify its displacement from the initial variational manifold.

Our results show that shallow NQS architectures trained with quantum natural gradient are particularly sensitive to this relocation. Depending on the rotation angle, optimization trajectories can be diverted toward saddle-point regions or high-curvature barriers of the loss manifold. In these cases, the network often achieves a small relative energy error while failing to reproduce the correct structure of the ground-state. To diagnose this mismatch, we supplement energy-based metrics with fidelity and coefficient Shannon entropy (quantum coherence) [18].

The distinction between ferromagnetic and antiferromagnetic regimes further highlights the role of spectral structure in shaping optimization dynamics. In the ferromagnetic case, near-degenerate low-energy eigenstates generate high-curvature regions in parameter space that can trap optimization at intermediate fidelities, whereas in the antiferromagnetic case, the closing of the excitation gap leads to different failure modes. Importantly, these effects arise even though the applied basis rotations do not alter entanglement measures derived from reduced density matrices, underscoring that entanglement alone is insufficient to characterize variational difficulty.

Beyond quantum many-body physics, our analysis connects naturally to broader questions in modern machine learning concerning optimization landscapes and information geometry [7, 26]. In contrast to typical supervised learning tasks that emphasize generalization, the NQS ground-state search is a high-precision regression problem on a fixed target functional, where convergence is governed by landscape curvature rather than overfitting behavior [10]. By leveraging analytically solvable models, we obtain direct insight into how representational constraints and information-geometric structure jointly influence optimization, complementing recent studies of variational quantum algorithms and neural-network ansätze [12, 16].

The paper is organized as follows. In Sec. II we introduce the basis-rotation framework and discuss relevant physical properties of the Ising ground state. In Sec. III we summarize the NQS architectures, loss functions, and optimization methods employed. In Sec. IV we analyze information-geometric considerations and potential pitfalls affecting optimization. Section V presents our numerical results, and Sec. VI discusses the broader implications of our findings for landscape-aware design of variational quantum algorithms.

II. BASIS ROTATION

To isolate how basis choice affects NQS optimization without altering the underlying physics, we study the

transverse-field Ising model on a ring:

$$H = J \sum_{i=1}^N \sigma_i^z \sigma_{i+1}^z + h \sum_{i=1}^N \sigma_i^x, \quad (1)$$

where σ^x and σ^z are the usual Pauli matrices and periodic boundary conditions identify site $N + 1 \equiv 1$. We then apply a local rotation around the y -axis at each site. The single-spin rotation operator is

$$U_y(\phi) = e^{i\phi\sigma^y} = \cos\phi I + i \sin\phi\sigma^y,$$

and the full N -spin rotation is

$$U_y^{(N)}(\phi) = [U_y(\phi)]^{\otimes N}.$$

Because U_y commutes with σ^y and rotates $\sigma^x \leftrightarrow \sigma^z$, it leaves the spectrum of H unchanged while transforming each eigenvector. In particular, if $|\psi_0\rangle$ is the ground state in the computational (σ^z) basis, then $|\psi_\phi\rangle = U_y^{(N)}(\phi)|\psi_0\rangle$ is the corresponding ground state in the rotated basis.

III. METHODS

In the following section we shortly summarize the standard NQS optimization procedure. We denote the network parameters by θ and represent the variational wavefunction $\psi_\theta(s)$ for spin configurations $s \in \{\pm 1\}^N$. We consider two shallow architectures. An RBM with N visible units and M hidden units models the log-amplitude as

$$\ln \psi_\theta(s) = \sum_{i=1}^N a_i s_i + \sum_{j=1}^M \ln \left[1 + \exp(b_j + \sum_{i=1}^N w_{ij} s_i) \right], \quad (2)$$

where $\theta = \{a_i, b_j, w_{ij}\}$ and the hidden-unit ratio $\alpha_{\text{RBM}} = M/N$ controls capacity. Because $\ln \psi_\theta(s) \in \mathbb{R}$, the resulting $\psi_\theta(s) = \exp[\ln \psi_\theta(s)]$ is nonnegative; capturing sign structures or phases requires introducing complex weights [9].

A fully connected network with L layers computes

$$f^{(\ell)}(y) = \tanh(W^{(\ell)}y + b^{(\ell)}), \quad (3)$$

$$\ln \psi_\theta(s) = f^{(L)}(f^{(L-1)}(\dots f^{(1)}(s))), \quad (4)$$

where θ collects all weights $\{W^{(\ell)}\}$ and biases $\{b^{(\ell)}\}$. The depth L and hidden-unit widths determine expressivity. FFNNs provide a flexible, architecture-agnostic representation that can, in principle, capture complex entanglement patterns beyond area-law constraints [13, 24]. In both architectures, the variational state is given as:

$$|\psi_\theta\rangle = \sum_s \psi_\theta(s) |s\rangle, \quad \psi_\theta(s) = \exp[\ln \psi_\theta(s)]. \quad (5)$$

Using log-amplitudes simplifies computation of log-derivatives (score functions):

$$O_k(s) = \partial_k \ln \psi_\theta(s), \quad \partial_k \psi_\theta(s) = O_k(s) \psi_\theta(s),$$

which are essential for gradient-based optimization in a high-dimensional parameter space [28].

We employ two loss functions for variational optimization, energy minimization:

$$E(\theta) = \frac{\langle \psi_\theta | H | \psi_\theta \rangle}{\langle \psi_\theta | \psi_\theta \rangle}, \quad (6)$$

where H is the Hamiltonian. Minimizing $E(\theta)$ corresponds to classical regression on the target energy functional but can converge to solutions with low energy error yet poor overlap with the true ground state, especially in near-degenerate regimes [16]. In the other case we use Infidelity Minimization:

$$I(\theta) = 1 - \frac{|\langle \psi_\theta | \psi_t \rangle|^2}{\langle \psi_\theta | \psi_\theta \rangle \langle \psi_t | \psi_t \rangle}, \quad (7)$$

where $|\psi_t\rangle$ is the exact ground state (available with ED). Minimizing $I(\theta)$ directly maximizes network fidelity but can become trapped near saddle points in a high-curvature loss manifold [12]. We use quantum natural gradient (stochastic reconfiguration), which preconditions $\nabla_\theta E$ with the inverse quantum Fisher information matrix $G(\theta)$. Information-geometrically, the Fubini–Study distance between two variational states $|\psi_\theta\rangle$ and $|\psi_{\theta+\delta\theta}\rangle$ is

$$d(\psi_\theta, \psi_{\theta+\delta\theta}) = \cos^{-1} \sqrt{\frac{\langle \psi_\theta | \psi_{\theta+\delta\theta} \rangle \langle \psi_{\theta+\delta\theta} | \psi_\theta \rangle}{\langle \psi_\theta | \psi_\theta \rangle \langle \psi_{\theta+\delta\theta} | \psi_{\theta+\delta\theta} \rangle}}. \quad (8)$$

For small $\delta\theta$,

$$d^2(\psi_\theta, \psi_{\theta+\delta\theta}) = \delta\theta^\dagger G(\theta) \delta\theta, \quad (9)$$

$$G_{ij}(\theta) = \frac{\langle \partial_i \psi_\theta | \partial_j \psi_\theta \rangle}{\langle \psi_\theta | \psi_\theta \rangle} - \frac{\langle \partial_i \psi_\theta | \psi_\theta \rangle \langle \psi_\theta | \partial_j \psi_\theta \rangle}{\langle \psi_\theta | \psi_\theta \rangle^2}. \quad (10)$$

This quantitative measure of local curvature on the parameter manifold ensures that updates follow steepest descent under the Fubini–Study metric [27]. The update rule becomes

$$\theta \mapsto \theta - \eta [G(\theta) + \epsilon I]^{-1} \nabla_\theta E,$$

where $\eta = 10^{-2}$ is the learning rate and $\epsilon = 10^{-6}$ regularizes the Fisher matrix inversion. This approach often accelerates convergence compared to naive gradient descent but can still stall if $G(\theta)$ becomes ill-conditioned near saddle points [12, 28].

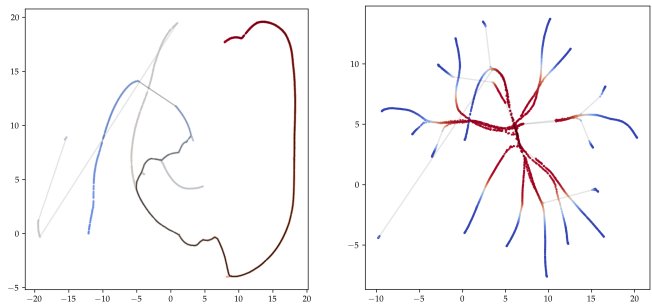


FIG. 1: UMAP projection of several NQS trajectories indicating different landscapes according to (6) and (7) respectively. Color denotes the infidelity with respect to the ground state of ferromagnetic Ising model with $N = 5, h = 0.5$

IV. CONSIDERATIONS

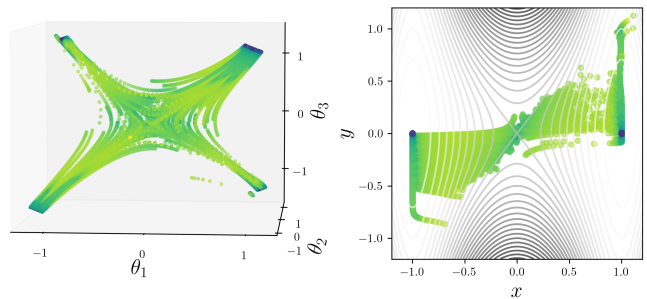


FIG. 2: Toy example of the smooth map defined in (11) that shows how the curvature and the saddle point occurring in the loss function space influences the parameter manifold Θ , causing another saddle point in the input space.

To discuss the performance of neural network learning in general, the most convenient setup arises naturally from differential geometry, which involves treating the network as a smooth map.

$$f : \Theta \mapsto \mathcal{Y}, \quad (11)$$

Let us for simplicity consider real parameters $\Theta \subset \mathbb{R}^P$ is the space of parameters θ and $\mathcal{Y} \subset \mathbb{R}^D$ is the output space [2]. An infinitesimal change $v \in T_\theta \Theta$ is carried forward by the pushforward (differential)

$$df_\theta(v) = \left. \frac{d}{dt} f(\theta + tv) \right|_{t=0},$$

which can be computed via a Jacobian-vector product (JVP) in automatic differentiation frameworks [5, 8]. Conversely, a cotangent vector $w \in T_{f(\theta)}^* \mathcal{Y}$ is pulled back to a covector on Θ by the pullback map

$$df_\theta^*(w) = w^\top \frac{\partial f}{\partial \theta}(\theta),$$

computed via a vector-Jacobian product (VJP). If \mathcal{Y} is endowed with a Riemannian metric G_y , then the pullback of G_y by f yields an induced metric g_θ on parameters given by

$$g_\theta(v, v) = \langle df_\theta(v), df_\theta(v) \rangle_{G_y} = v^\top J(\theta)^\top G_y J(\theta) v,$$

where $J(\theta) = \frac{\partial f}{\partial \theta}(\theta)$ is the Jacobian [23]. In particular, when the loss is a function $\ell : \mathcal{Y} \rightarrow \mathbb{R}$ and one considers the composite $L(\theta) = \ell(f(\theta))$, the gradient $\nabla_\theta L$ is precisely the pullback of the differential $d\ell \in T_{f(\theta)}^* \mathcal{Y}$ via df_θ^* , yielding

$$\nabla_\theta L = \left(\frac{\partial f}{\partial \theta}(\theta) \right)^\top \nabla_y \ell,$$

which follows from the chain rule in information geometry [23]. The natural gradient method uses this induced metric g_θ (often instantiated as the Fisher information matrix) to precondition the ordinary gradient:

$$\tilde{\nabla} L(\theta) = g_\theta^{-1} \nabla_\theta L,$$

corresponding to steepest descent in the parameter manifold endowed with the pullback (Fisher–Rao) metric, making updates invariant to smooth reparameterizations [3, 21]. Thus, pushforwards capture how parameter perturbations propagate to outputs via JVP, pullbacks capture how output-space gradients and metrics induce geometric structure on the parameter manifold via VJP, and the natural gradient exploits this geometry to perform reparameterization-invariant optimization [3]. Therefore it is easy to see that the perspective of the pullback allows us to consider the neural network learning as a dual trajectory on both the parameter manifold and the output space. The optimizer therefore provides the information for the network on how and where to move in the variational landscape. Neural quantum states (NQS) were first introduced by Carleo and Troyer as a variational ansatz for quantum many-body wavefunctions, where a neural network with parameters W outputs the complex amplitude $\langle \mathbf{s} | \Psi; W \rangle$ for each configuration $\mathbf{s} = (s_1, \dots, s_N)$ [9]. This defines a smooth map

$$f_{\text{NQS}} : M \longrightarrow \mathbb{C}^{2^N},$$

with $M \subset \mathbb{R}^P$ the space of neural-network parameters. In parallel, tensor-network ansätze (e.g., matrix product states or correlator product states) and variational quantum circuits (VQE) also realize smooth maps

$$f_{\text{TN}}, f_{\text{VQE}} : M \longrightarrow \mathbb{C}^{2^N},$$

where $f_{\text{VQE}}(\theta)$ is the state produced by a parametrized quantum circuit $U(\theta)$ acting on a reference state $|0\rangle^{\otimes N}$ [20]. By treating these models uniformly as $f : M \rightarrow \mathbb{C}^{2^N}$, one sees that any infinitesimal move $v \in T_\theta M$ on the parameter manifold pushes forward to a change in the quantum state $df_\theta(v) \in T_\psi \mathcal{H}$. Given an infidelity loss

$$L(\theta) = 1 - |\langle \psi(\theta) | \phi \rangle|^2,$$

where $|\phi\rangle$ is a target state (e.g., ground state in VQE), its differential $dL \in T_{\psi(\theta)}^* \mathcal{H}$ is pulled back by

$$df_\theta^* : T_{|\psi(\theta)\rangle}^* \mathcal{H} \longrightarrow T_\theta^* M,$$

so that the gradient in parameter space satisfies

$$\nabla_\theta L = (J(\theta))^\dagger \nabla_\psi L = (J(\theta))^\dagger (-\langle \phi | \psi(\theta) \rangle \langle \phi |),$$

where $J(\theta) = \partial f / \partial \theta$ is the Jacobian of the map f [1, 20]. The projective Hilbert space of N -qubit pure states, $\mathbb{C}P^{2^N-1}$, is a Kähler manifold equipped with the Fubini–Study metric G_{FS} , whose line element for two infinitesimally close normalized states $|\psi\rangle$ and $|\psi + d\psi\rangle$ is

$$ds^2 = 1 - |\langle \psi | \psi + d\psi \rangle|^2.$$

When a parametrized map $f : M \rightarrow \mathbb{C}^{2^N}$ is introduced, this metric pulls back to the parameter manifold as

$$\begin{aligned} g_\theta^{FS}(v, v) &= \langle df_\theta(v), df_\theta(v) \rangle_{FS} & (12) \\ &= v^\dagger J(\theta)^\dagger J(\theta) v - |\langle \psi(\theta) | J(\theta) v \rangle|^2, & (13) \end{aligned}$$

which coincides with the quantum geometric tensor’s real part, i.e., the quantum Fisher information metric for pure states [13]. Under an infidelity loss $L(\theta) = 1 - |\langle \psi(\theta) | \phi \rangle|^2$, the natural gradient

$$\tilde{\nabla} L(\theta) = (g_\theta^{FS})^{-1} \nabla_\theta L$$

yields updates that follow steepest descent along geodesics of $\mathbb{C}P^{2^N-1}$ pulled back to M , ensuring that small steps in parameter space correspond to minimal fidelity loss in state space. Because VQE, tensor-network ansätze, and NQS share the same mathematical structure as smooth maps $f : M \rightarrow \mathbb{C}^{2^N}$, one can directly apply geometric optimization techniques—particularly quantum natural gradient descent—across all these variational paradigms. In each case, the pullback of the Fubini–Study metric defines a Riemannian manifold structure on M , and the infidelity loss naturally corresponds to the squared geodesic distance on $\mathbb{C}P^{2^N-1}$. Hence, by measuring the Fubini–Study distance between $|\psi(\theta)\rangle$ and the target $|\phi\rangle$, the optimizer gains geometric information about “how and where to move” in the variational landscape—exactly as was noted for classical neural networks, but now elevated to the quantum wavefunction manifold [20].

In this way, one easily sees that treating M as the parameter space and \mathbb{C}^{2^N} (up to normalization and global phase) as the output statevector space allows a unified geometric framework for VQE, tensor networks, and neural quantum states. Directly measuring the Fubini–Study distance in state space under an infidelity-based loss establishes a well-defined loss manifold whose metric

structure is given by the pullback g_θ^{FS} . This geometric setup ensures that natural gradient optimization inherently accounts for quantum-information-theoretic distances, leading to more efficient and stable convergence across all these variational quantum algorithms.

A. Physical Considerations

In particular, we can directly compare the information-geometric distance (e.g., via Fubini–Study metrics) between a typical random initialization and $|\psi_\phi\rangle$, and thereby quantify how basis rotation affects the optimization trajectory.

Neural network parameters are typically initialized randomly near zero, which yields an initial state close to the equal-weight superposition

$$|W\rangle = \frac{1}{\sqrt{2^N}} \sum_{s \in \{\pm 1\}^N} |s\rangle.$$

To remove initialization noise, we first pretrain each model to represent $|W\rangle$ by minimizing its infidelity. Once convergence is achieved (infidelity $< 10^{-8}$), these parameters serve as a common, exact initialization for all subsequent runs. This ensures that differences in convergence arise solely from model–landscape interactions rather than random initialization.

B. Pitfalls

Several pitfalls can obscure genuine model performance:

1. **Sampling Noise** - Although Monte Carlo sampling is common in large-scale NQS, here we avoid it by restricting to $N < 20$, ensuring exact gradient and expectation evaluation.
2. **Architecture Limitations** - Shallow RBMs and small FFNNs may lack the expressivity required to represent complex rotated states. Tuning the hidden-unit ratio ($\alpha_{\text{RBM}} = M/N$) or network depth is crucial, but even well-tuned shallow models can stall when the target lies in a high-curvature region.
3. **Loss-Function Traps** - Energy minimization can lead to low-energy states that still have poor fidelity. Conversely, minimizing infidelity directly can become trapped near saddles, as optimization steps shrink in high-curvature valleys. Figure 1 shows trajectories under both losses, highlighting these challenges.
4. **Quantum Natural Gradient Conditioning** - The quantum Fisher matrix $G(\alpha)$ can become ill-conditioned in narrow valleys or near saddles, causing updates to stall or oscillate. Regularization (ϵI)

mitigates this but does not fully eliminate saddle-point trapping.

5. **Initialization Bias** - Starting from a random initialization often places the model near the equal-weight superposition $|W\rangle$. Without pretraining, different random seeds can yield diverse trajectories. By pretraining to $|W\rangle$, we fix a deterministic initialization, isolating the effect of rotated targets on convergence.

By addressing these pitfalls we ensure that observed differences in training performance reflect intrinsic challenges of the fixed loss landscape and the rotated ground-state location rather than extraneous artifacts.

V. RESULTS

In Figures 5 we use the relative energy error $\epsilon_{\text{rel}} = |(E_{\text{NQS}} - E_{\text{exact}})/E_{\text{exact}}|$ as our figure of merit. Comparing the cases $J = \pm 1$ allows us to study two models with same inherent symmetries but different spectra: the gapped ferromagnetic case ($J = -1$) and the gapless antiferromagnetic case ($J = +1$). In the ferromagnetic case, the gap between the two lowest eigenstates decays exponentially, whereas in the antiferromagnetic case, the $2N$ -fold band closes algebraically.

Let us first compare the antiferromagnetic case (Upper three subplots of) which indicates that for larger systems sizes $L > 5$ RBM fails to converge for all angles except special points $\theta_k = 0, \pi/2, \pi$. On the other hand, one can observe that the ferromagnetic case (lower three subplots of) seems to exhibit higher accuracy and a flat angle dependence with larger standard deviation again for angles θ_k and furthermore that the relative energy error appears to decrease with system size. But this is actually misleading, as by inspecting more closely the infidelity, the accuracy actually does not decrease below $1 - \mathcal{F} = 0.5$, rather the energy gap between between two lowest energies decreases. And this tells us an important thing about sensitivity of NQS on the eigen-spectrum of the Hamiltonian.

Rotating the basis does not change entanglement measures that depend only on the spectrum of reduced density matrices; for example, the entanglement entropy of any bipartition is identical for $|\psi_0\rangle$ and $|\psi_\phi\rangle$. To assess how “far” the rotated wavefunction sits from typical NQS initializations, we instead monitor quantities that depend on the full statevector in the rotated basis. In this case we use quantum coherence as the Shannon entropy of the wavefunction’s coefficients in the rotated basis. Since $U_y(\phi)$ mixes $|0\rangle$ and $|1\rangle$ at each site, the rotated ground state often acquires a nontrivial distribution of amplitudes, and its coherence can increase relative to the unrotated case. By tracking how these resource measures vary with ϕ , we gain insight into how much “harder” the rotated ground state is for a given NQS ansatz to represent.

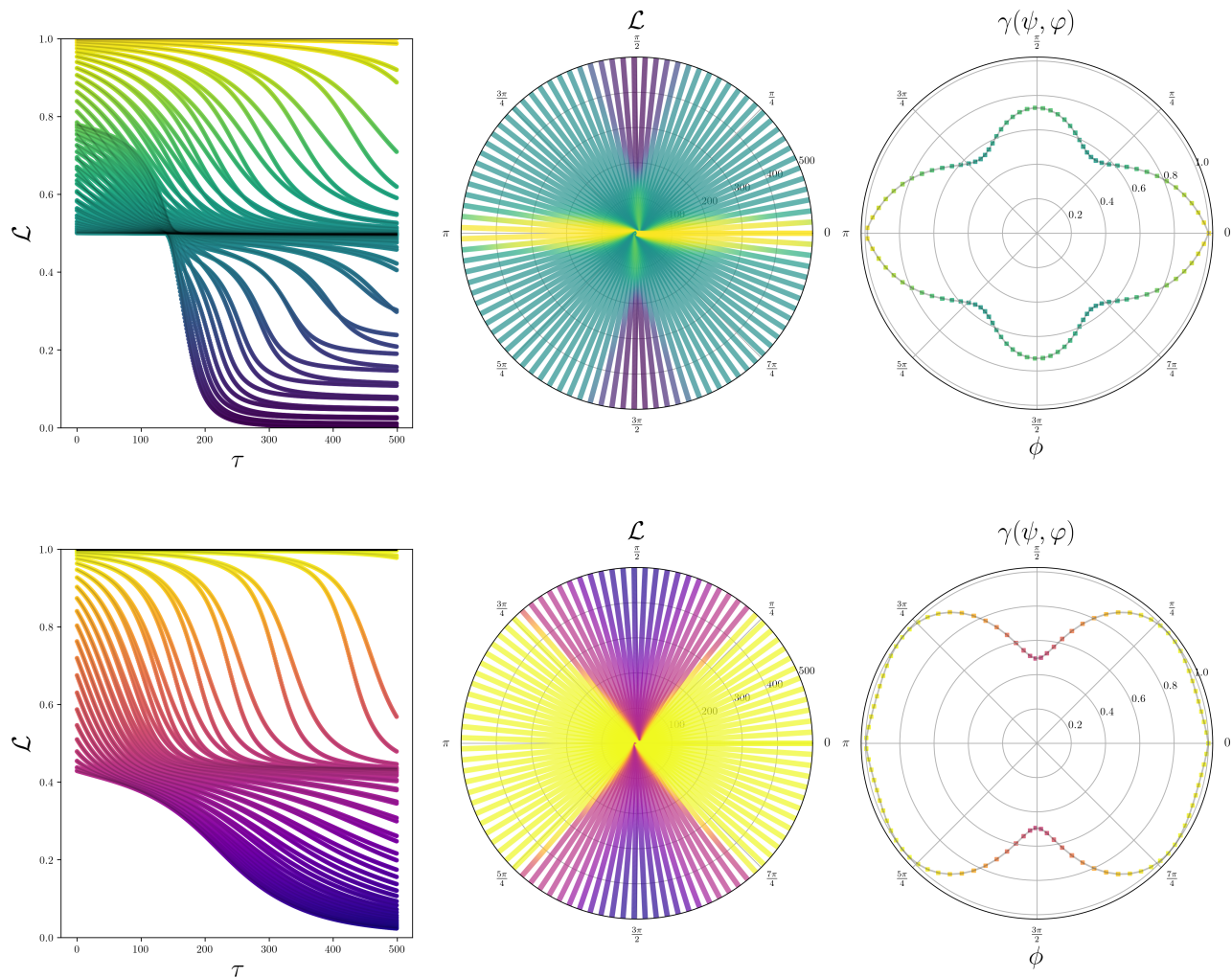


FIG. 3: Comparison of Fubini Study Distance γ and Loss \mathcal{L} from NQS trained with infidelity minimization up to initial state $|\psi\rangle = 1/\sqrt{2^N} \sum_{s \in \{\pm 1\}^N} |s\rangle$ and then to the target rotated state ground state $|\varphi(\phi)\rangle$ for $N = 5, h = 0.5$ with $J = -1$ (top) and $J = +1$ (bottom) as function of rotation angle ϕ .

The proposed rotation of the target state increases the chance of NQS to get trapped in a saddle point (see Figure 7).

The importance of the proliferation of saddle points and the connection to computational complexity provided in Sec. IV can be showcased in the comparison of different algorithms (see Figure 4).

VI. CONCLUSION AND DISCUSSION

In this work, we explored how local basis rotations in a one-dimensional transverse Ising model affect the convergence of Neural Quantum States without altering the underlying loss landscape. By applying sitewise rotations parameterized by θ , we moved the exact ground-state wavefunction within a fixed optimization landscape and evaluated how shallow ansätze—particularly

Restricted Boltzmann Machines and small feedforward networks—trained with quantum natural gradient respond. Our results show that, although the energy spectrum remains unchanged, the rotated wavefunction’s information-geometric distance from typical initializations increases, making it more difficult for shallow NQS to reach the true ground state. In the ferromagnetic case, near-degenerate eigenstates produce high-curvature barriers that manifest as saddle points; as a consequence, the network often converges to a low-energy superposition that fails to reproduce correct coefficient statistics despite a small relative energy error. Across all rotation angles and both ferromagnetic and antiferromagnetic regimes, these phenomena highlight the sensitivity of NQS optimization to the location of the ground state in parameter space.

Several practical implications emerge from our findings. First, basis rotations that leave the loss landscape

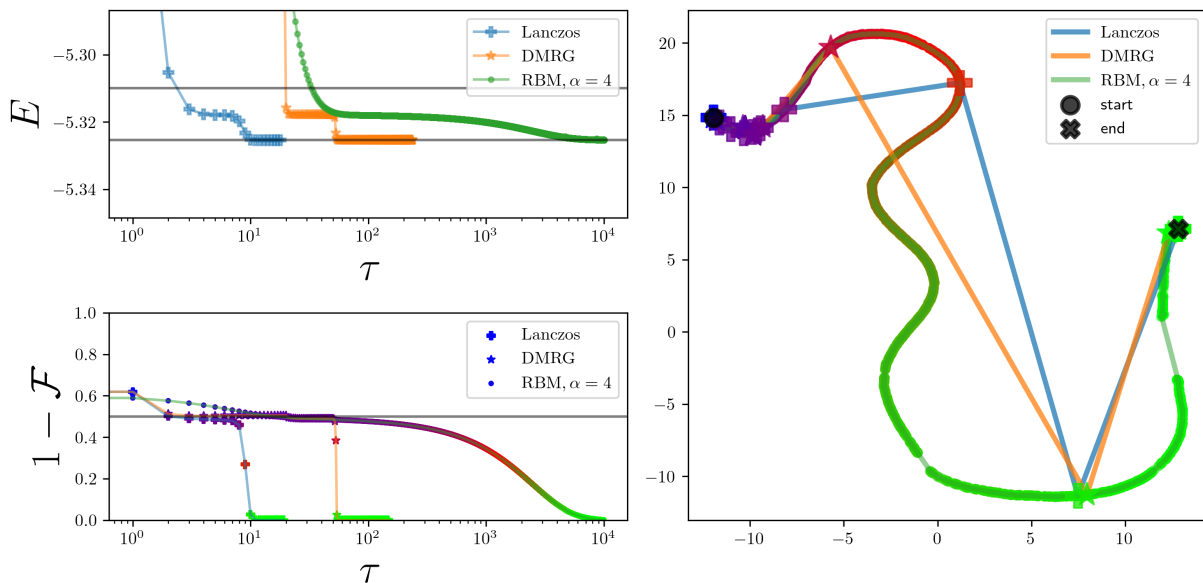


FIG. 4: Discussion in Sec. IV can help us unify the understanding in variational optimization of different algorithms. In this case we compare the performance of Lanczos algorithm [19], DMRG and RBM with $\alpha = 4$ starting from the same initial statevector and the ferromagnetic Ising model $N = 5, h = -0.5, \phi = \pi/3$. Left top plot shows energy E during iterations τ while bottom plot paints the colormap for infidelity $1 - \mathcal{F}$. All three algorithms encounter the same saddle point region. The right plot compares the corresponding statevector trajectories using UMAP projection.

invariant can nonetheless degrade performance by relocating the target into regions with unfavorable curvature—regions where quantum natural gradient updates may stall. Second, shallow architectures that perform well near the computational basis exhibit significant degradation when tasked with representing rotated states of higher “magic” or coherence. Third, minimizing infidelity rather than energy can help focus training on overlap with the exact state, but it does not fully eliminate saddle-point trapping for rotated targets. Taken together, these observations underscore the importance of aligning ansatz expressivity and initialization strategies with the expected information-geometric properties of the target wavefunction.

Looking forward, our study suggests several avenues for improving variational approaches. More expressive architectures—such as deeper feedforward networks or convolutional structures—may better navigate high-curvature regions and represent rotated states with larger quantum resources. Adaptive scheduling of quantum natural gradient regularization or hybrid loss functions that combine energy and infidelity could help avoid suboptimal basins. Finally, analytically solvable models like the rotated Ising chain offer a valuable testbed for diagnosing optimization challenges, enabling more systematic investigations of landscape geometry and guiding the design of robust, interpretable variational algorithms for complex quantum systems.

ACKNOWLEDGEMENT

SBK thanks Gianpaolo Torre and Jovan Odavić for the help and support, and also thanks Miha Srdinšek

and Sidhartha Shankar Dash for insightful discussions related to problems encountered with variational optimization. SBK acknowledges discussions with Roberto Verdel on related aspects of NQS basis dependency as well. VZ acknowledges support and funding by Croatian Science Foundation (HrZZ) project IP-2022-10-1648. SBK, FF and SMG acknowledge support from the project “Implementation of cutting-edge research and its application as part of the Scientific Center of Excellence for Quantum and Complex Systems, and Representations of Lie Algebras”, Grant No. PK.1.1.10.0004, co-financed by the European Union through the European Regional Development Fund - Competitiveness and Cohesion Programme 2021- 2027. SBK acknowledges support from the Croatian Science Foundation (HrZZ) Projects DOK-2020-01-9938.

VII. DATA AND CODE AVAILABILITY

Data and codes are available upon request to the authors. Some of the simulations were partially performed using the open source Netket library [29, 30], while majority used custom adapted codes in Jax framework [8].

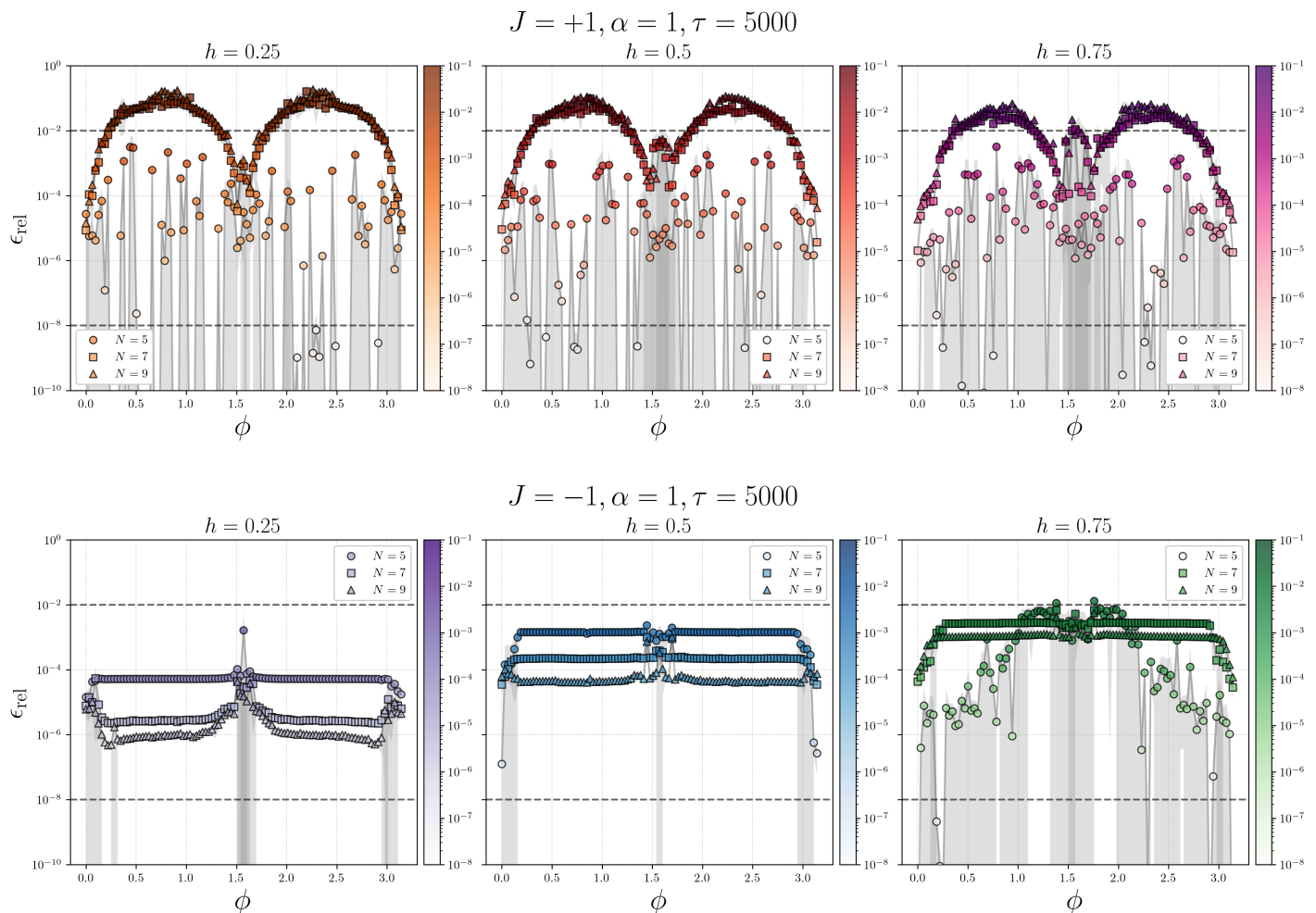


FIG. 5: Relative Error versus angle of rotation ϕ for logRBM ($\alpha = 1$) with SR for $\tau = 5000$ iterations for rotated $H(\phi) = U_\phi H U_\phi^\dagger$ (1)

-
- [1] Amira Abbas, David Sutter, Christa Zoufal, Aurelien Lucchi, Alessio Figalli, and Stefan Woerner. The power of quantum neural networks. *Nature Computational Science*, 1(6):403–409, June 2021. ISSN 2662-8457. doi:10.1038/s43588-021-00084-1. URL <http://dx.doi.org/10.1038/s43588-021-00084-1>.
- [2] S. Amari and H. Nagaoka. *Methods of Information Geometry*. Translations of mathematical monographs. American Mathematical Society, 2000. ISBN 9780821843024.
- [3] Shun-ichi Amari. Natural gradient works efficiently in learning. *Neural Computation*, 10(2):251–276, 02 1998. ISSN 0899-7667. doi:10.1162/089976698300017746. URL <https://doi.org/10.1162/089976698300017746>.
- [4] Rodney J. Baxter. *Exactly Solved Models in Statistical Mechanics*. Academic Press, London, 1982. doi:10.1142/9789814415255_0002.
- [5] Atılım Güneş Baydin, Barak A. Pearlmutter, Alexey Andreyevich Radul, and Jeffrey Mark Siskind. Automatic differentiation in machine learning: a survey. *J. Mach. Learn. Res.*, 18(1):5595–5637, January 2017. ISSN 1532-4435.
- [6] Federico Becca and Sandro Sorella. *Quantum Monte Carlo Approaches for Correlated Systems*. Cambridge University Press, 2017. doi:10.1017/9781316417041.
- [7] Mikhail Belkin, Daniel Hsu, Siyuan Ma, and Soumik Mandal. Reconciling modern machine-learning practice and the classical bias–variance trade-off. *Proceedings of the National Academy of Sciences*, 116(32):15849–15854, July 2019. ISSN 1091-6490. doi:10.1073/pnas.1903070116. URL <http://dx.doi.org/10.1073/pnas.1903070116>.
- [8] James Bradbury, Roy Frostig, Peter Hawkins, Matthew James Johnson, Chris Leary, Dougal Maclaurin, George Necula, Adam Paszke, Jake VanderPlas, Skye Wanderman-Milne, and Qiao Zhang. JAX: composable transformations of Python+NumPy programs, 2018. URL <http://github.com/google/jax>.

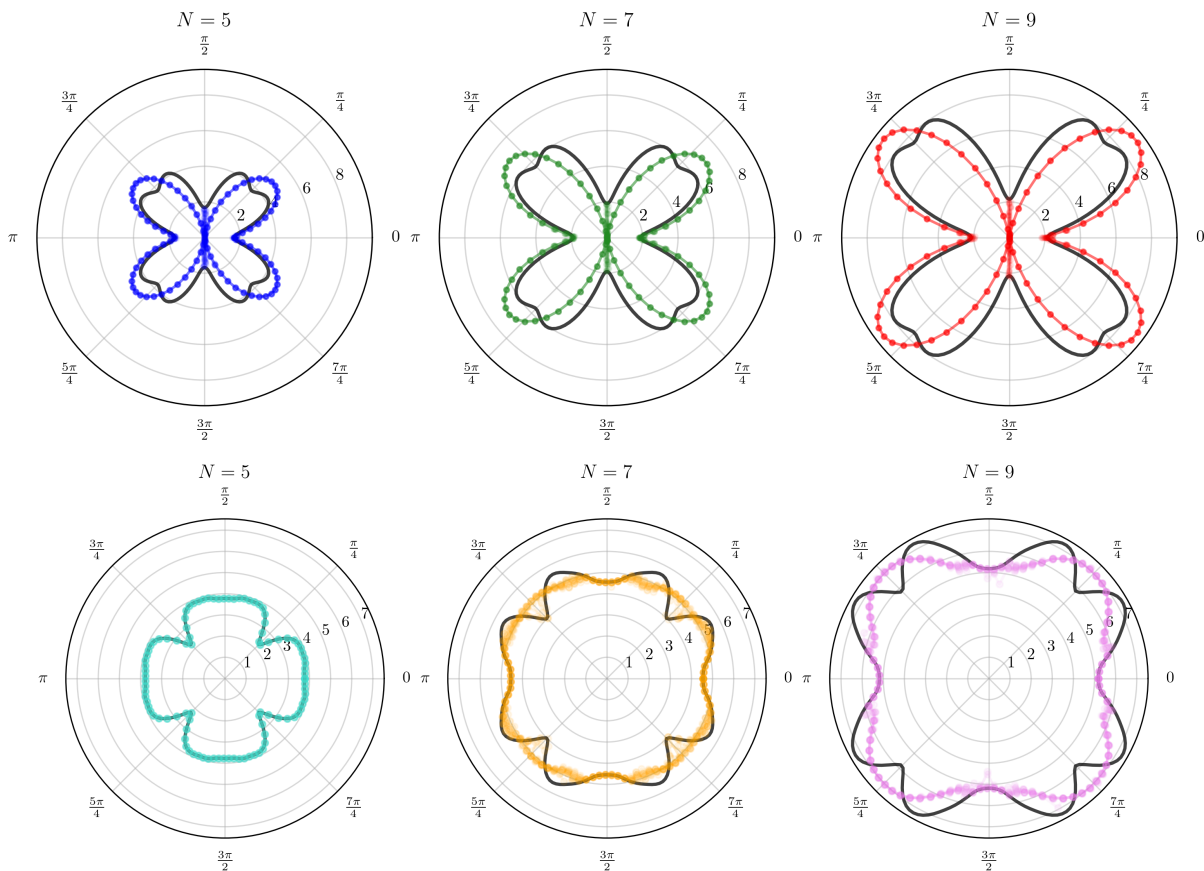


FIG. 6: Shannon entropy of variational state-vector coefficients (Quantum Coherence) of logRBM ($\alpha = 1$) with SR for $\tau = 5000$ iterations, $h = 0.5$, $N = 5, 7, 9$, with $J = -1$ (top) and $J = +1$ (bottom) as function of rotation angle ϕ

- [9] Giuseppe Carleo and Matthias Troyer. Solving the quantum many-body problem with artificial neural networks. *Science*, 355(6325):602–606, February 2017. ISSN 1095-9203. doi:10.1126/science.aag2302. URL <http://dx.doi.org/10.1126/science.aag2302>.
- [10] Ao Chen and Markus Heyl. Empowering deep neural quantum states through efficient optimization. *Nature Physics*, 20(9):1476–1481, July 2024. ISSN 1745-2481. doi:10.1038/s41567-024-02566-1. URL <http://dx.doi.org/10.1038/s41567-024-02566-1>.
- [11] Ronald Santiago Cortes, Aravindh S. Shankar, Marcello Dalmonte, Roberto Verdel, and Nils Niggemann. Basis dependence of neural quantum states for the transverse field ising model, 2025. URL <https://arxiv.org/abs/2512.11632>.
- [12] Sidhartha Dash, Luca Gravina, Filippo Vicentini, Michel Ferrero, and Antoine Georges. Efficiency of neural quantum states in light of the quantum geometric tensor. *Communications Physics*, 8(1), March 2025. ISSN 2399-3650. doi:10.1038/s42005-025-02005-4. URL <http://dx.doi.org/10.1038/s42005-025-02005-4>.
- [13] Dong-Ling Deng, Xiaopeng Li, and S. Das Sarma. Quantum entanglement in neural network states. *Phys. Rev. X*, 7:021021, May 2017. doi:10.1103/PhysRevX.7.021021. URL <https://link.aps.org/doi/10.1103/PhysRevX.7.021021>.
- [14] Zakari Denis, Alessandro Sinibaldi, and Giuseppe Carleo. Comment on “can neural quantum states learn volume-law ground states?”. *Physical Review Letters*, 134(7), February 2025. ISSN 1079-7114. doi:10.1103/physrevlett.134.079701. URL <http://dx.doi.org/10.1103/PhysRevLett.134.079701>.
- [15] Fabio Franchini. *An Introduction to Integrable Techniques for One-Dimensional Quantum Systems*. Springer, Cham, 2017. doi:10.1007/978-3-319-48487-7.
- [16] Clemens Giuliani, Filippo Vicentini, Riccardo Rossi, and Giuseppe Carleo. Learning ground states of gapped quantum hamiltonians with kernel methods. *Quantum*, 7:1096, August 2023. ISSN 2521-327X. doi:10.22331/q-2023-08-29-1096. URL <http://dx.doi.org/10.22331/q-2023-08-29-1096>.
- [17] W. Kohn and L. J. Sham. Self-consistent equations including exchange and correlation effects. *Phys. Rev.*, 140:A1133–A1138, Nov 1965. doi:10.1103/PhysRev.140.A1133. URL <https://link.aps.org/doi/10.1103/PhysRev.140.A1133>.
- [18] Sven Benjamin Kožić and Gianpaolo Torre. Computing quantum resources using tensor cross interpolation, 2025. URL <https://arxiv.org/abs/2502.06956>.
- [19] Cornelius Lanczos. An iteration method for the solution of the eigenvalue problem of linear differential and integral operators. *J. Res. Natl. Bur. Stand. B*, 45:255–282, 1950. doi:10.6028/jres.045.026.

- [20] Martín Larocca, Nathan Ju, Diego García-Martín, Patrick J. Coles, and Marco Cerezo. Theory of overparametrization in quantum neural networks. *Nature Computational Science*, 3(6):542–551, June 2023. ISSN 2662-8457. doi:10.1038/s43588-023-00467-6. URL <http://dx.doi.org/10.1038/s43588-023-00467-6>.
- [21] James Martens. New insights and perspectives on the natural gradient method. *Journal of Machine Learning Research*, 21(146):1–76, 2020. URL <http://jmlr.org/papers/v21/17-678.html>.
- [22] Román Orús. A practical introduction to tensor networks: Matrix product states and projected entangled pair states. *Annals of Physics*, 349:117–158, 2014. doi:10.1016/j.aop.2014.06.013.
- [23] Razvan Pascanu and Yoshua Bengio. Revisiting natural gradient for deep networks, 2014. URL <https://arxiv.org/abs/1301.3584>.
- [24] Giacomo Passetti, Damian Hofmann, Pit Neiteimer, Lukas Grunwald, Michael A. Sentef, and Dante M. Kennes. Can neural quantum states learn volume-law ground states? *Phys. Rev. Lett.*, 131:036502, Jul 2023. doi:10.1103/PhysRevLett.131.036502. URL <https://link.aps.org/doi/10.1103/PhysRevLett.131.036502>.
- [25] Michael Y. Pei and Stephen R. Clark. Neural-network quantum states for spin-1 systems: Spin-basis and parameterization effects on compactness of representations. *Entropy*, 23(7):879, July 2021. ISSN 1099-4300. doi:10.3390/e23070879. URL <http://dx.doi.org/10.3390/e23070879>.
- [26] Daniel A. Roberts, Sho Yaida, and Boris Hanin. The principles of deep learning theory: An effective theory approach to understanding neural networks. May 2022. doi:10.1017/9781009023405. URL <http://dx.doi.org/10.1017/9781009023405>.
- [27] James Stokes, Josh Izaac, Nathan Killoran, and Giuseppe Carleo. Quantum natural gradient. *Quantum*, 4:269, May 2020. ISSN 2521-327X. doi:10.22331/q-2020-05-25-269. URL <http://dx.doi.org/10.22331/q-2020-05-25-269>.
- [28] Filippo Vicentini, Damian Hofmann, Attila Szabó, Dian Wu, Christopher Roth, Clemens Giuliani, Gabriel Pescia, Jannes Nys, Vladimir Vargas-Calderón, Nikita Astrakhantsev, and Giuseppe Carleo. NetKet 3: Machine learning toolbox for many-body quantum systems. *SciPost Physics Codebases*, aug 2022. doi:10.21468/scipostphyscodeb.7.
- [29] Filippo Vicentini, Damian Hofmann, Attila Szabó, Dian Wu, Christopher Roth, Clemens Giuliani, Gabriel Pescia, Jannes Nys, Vladimir Vargas-Calderón, Nikita Astrakhantsev, and Giuseppe Carleo. NetKet 3: Machine Learning Toolbox for Many-Body Quantum Systems. *SciPost Phys. Codebases*, page 7, 2022. doi:10.21468/SciPostPhysCodeb.7. URL <https://scipost.org/10.21468/SciPostPhysCodeb.7>.
- [30] Filippo Vicentini, Damian Hofmann, Attila Szabó, Dian Wu, Christopher Roth, Clemens Giuliani, Gabriel Pescia, Jannes Nys, Vladimir Vargas-Calderón, Nikita Astrakhantsev, and Giuseppe Carleo. Codebase release 3.4 for NetKet. *SciPost Phys. Codebases*, pages 7–r3.4, 2022. doi:10.21468/SciPostPhysCodeb.7-r3.4. URL <https://scipost.org/10.21468/SciPostPhysCodeb.7-r3.4>.
- [31] Tai-Hsuan Yang, Mehdi Soleimanifar, Thiago Bergamaschi, and John Preskill. When can classical neural networks represent quantum states?, 2024. URL <https://arxiv.org/abs/2410.23152>.

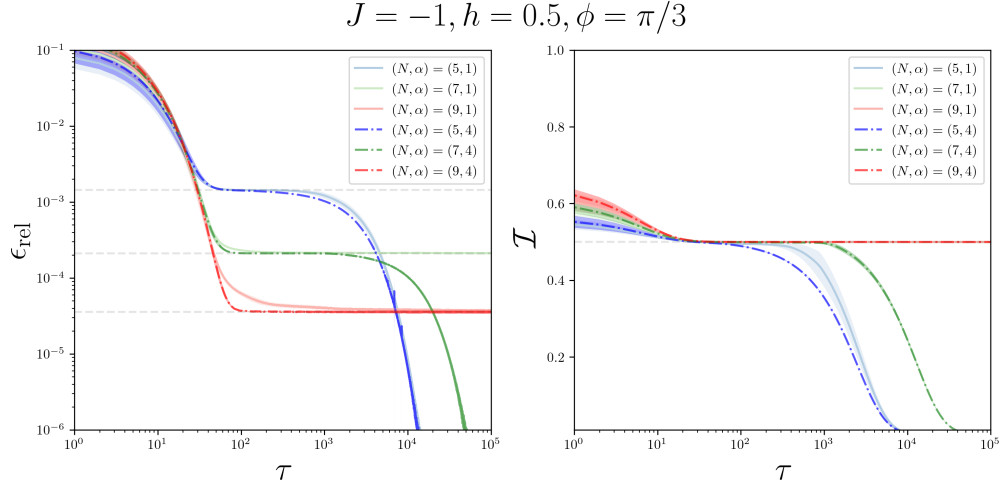


FIG. 7: Log-Log plot of averaged relative energy error for 10 samples for $N = 5, 7, 9$ with logRBM architecture ($\alpha = 4$) for $\tau = 10^5$ iterations of stochastic reconfiguration optimization, $\eta = 1e - 2, \delta = 1e - 6$. The horizontal lines indicate the relative error between exact ground state energy and the first excited energy divided by 2, indicating exact saddle point location.